Hao et al. EURASIP Journal on Advances in Signal Processing (2015) 2015:64
DOI 10.1186/s13634-015-0248-4

EURASIP Journal on Advances in Signal Processing
a SpringerOpen Journal

RESEARCH Open Access

Multiple-Symbol combined differential detection for satellite-based AIS Signals

Jingsong Hao*, Shexiang Ma, Junfeng Wang and Xin Meng

Abstract

In this paper, a multiple-symbol combined differential Viterbi decoding algorithm which is insensitive to frequency offset is proposed. According to the theories of multiple-symbol differential detection and maximum-likelihood detection, we combine the multiple-order differential information with the Viterbi algorithm. The phase shift caused by the frequency offset is estimated and compensated from the above information in the process of decoding. The simulation results show that the bit error rate (BER) of 2 bits combined differential Viterbi algorithm is below 10^{-3} when the normalized signal-to-noise ratio (NSNR) is 11 dB, and the decoding performances approach those of the coherent detection as the length of the combined differential symbols increases. The proposed method is simple and its performance remains stable under different frequency offsets.

Keywords: Automatic Identification System (AIS); Satellite; Multiple-symbol differential detection; Viterbi algorithm

1 Introduction

Automatic Identification System (AIS) [1], as a new type of navigation and security ensuring system on the sea, can realize ship-to-ship and ship-to-shore station communications well. Each ship equipped with AIS transmitter periodically sends status messages in the maritime very high frequency (VHF). Each AIS receiver nearby can receive these messages and provides a map of the local maritime traffic, thus, avoiding collisions on the sea. However, the AIS system was initially developed to realize horizon communication, so it has a limited coverage range [2]. The satellite-based AIS system receives messages from a constellation of low earth orbit satellites, which extends the range of coverage and attracts attention from more and more countries [3].

The satellite-based AIS system has large frequency offset so it is hard to recover the local carrier accurately [4]. Noncoherent sequence detection, which has simple structure and good performance without accurate local carrier, is optimal for receivers. A Viterbi decoding algorithm based on Laurent decomposition, which has a performance approaches that of coherent detection at the cost of high complexity, is proposed in [5]. A sequence estimation algorithm for the differential detection of the continuous phase modulation signals, which has significant gains in bit error rate (BER) performance and with considerable resistivity to fading, is introduced in [6]. A multiple differential detection (MDD) sequence estimator, which uses a decision feedback for the demodulation of Gaussian minimum shift keying (GMSK) signals, is described in [7]. A noncoherent GMSK detector using differential phase detection combined with the soft-output Viterbi algorithm (SOVA), which overcomes the severe intersymbol interference (ISI) of GMSK signals with low B_tT, is presented in [8]. The schemes mentioned before can achieve good performances, but their performances remain stable only within a certain range of frequency offset. When the frequency offset exceeds the range, it needs to be estimated and compensated. An innovative receiver architecture for the satellite-based AIS, which adopts the Viterbi decoding algorithm based on Laurent decomposition in [5], is described in [2]. A highly efficient receiver, which modifies the synchronization and detection algorithms in [2] and achieves an impressive performance improvement, is proposed in [9]. Both receivers adopt noncoherent detection algorithms and achieve good performances, but they need frequency synchronization before detection. The multiple-symbol differential detection (MSDD) of M-ary phase shift keying (MPSK) signals in the presence of frequency offset is studied in [10–12], which introduce a double differential

* Correspondence: jessonhao@163.com
School of Computer and Communication Engineering, Tianjin University of Technology, Tianjin 300384, China

MPSK modulation to realize the robustness to both frequency and phase offsets. Their format of the transmitted signals is changed. But the modulation system of AIS signal has been defined in [1], so the double differential encoding can't be applied to the detection for satellite-based AIS signals.

In this paper, we first introduce the baseband signal model and phase states of AIS signal. Then, a multiple-symbol combined differential detection algorithm base on the theories of multiple-symbol differential detection and maximum-likelihood detection is proposed. The phase shift caused by the frequency offset is estimated and compensated from the multiple-order combined differential information in the process of decoding. Finally, the decoding process is completed adopting Viterbi algorithm. The performance of the proposed algorithm over an AWGN channel is evaluated through computer simulation. The results show that this algorithm has good performance over AWGN channel and is insensitive to frequency offset and constant phase shift.

2 AIS baseband signal model and phase states

AIS baseband signal adopts GMSK modulation whose complex envelope [13] can be expressed as

$$s(t) = \sqrt{\frac{2E}{T_b}} e^{j\theta(t)} \tag{1}$$

where E is the signal energy per information symbol, T_b is the symbol period, and $\theta(t)$ is the phase of the modulating signal.

The phase of the GMSK modulating signal $\theta(t)$ can be expressed as

$$\theta(t) = \pi \sum_i a_i q(t - iT_b) \tag{2}$$

$$q(t) = \int_{-\infty}^{t} g(\tau) d\tau \tag{3}$$

$$g(t) = \frac{1}{2}\left\{ erfc\left[\frac{2\pi B}{\sqrt{2\ln 2}}\left(t - \frac{T_b}{2}\right)\right] - erfc\left[\frac{2\pi B}{\sqrt{2\ln 2}}\left(t + \frac{T_b}{2}\right)\right]\right\} \tag{4}$$

where $\{a_i\}$ is the information sequence, $g(t)$ is the frequency pulse, $q(t)$ is the phase-smoothing pulse response, and B is the 3 dB bandwidth of the Gaussian filter.

Theoretically speaking, the frequency pulse $g(t)$ is infinite. Considering its physical realization, we truncate it to L bits.

Substituting Eq. 4 into Eq. 3, it can be rewritten as

$$q(t) = \begin{cases} 0, & t < -\dfrac{(L-1)T_b}{2} \\ \dfrac{1}{2T_b}\displaystyle\int_{-\infty}^{t} g\left(\tau - \frac{1}{2}T_b\right) d\tau, & -\dfrac{(L-1)T_b}{2} \le t \le \dfrac{(L+1)T_b}{2} \\ \dfrac{1}{2}, & t > \dfrac{(L+1)T_b}{2} \end{cases} \tag{5}$$

Substituting Eq. 5 into Eq. 2 when $nT_b \le t \le (n+1)T_b$, it can be rewritten as

$$\begin{aligned} \theta(t) &= \pi \sum_{k=n-(L+1)/2+1}^{n+(L-1)/2} a_k q(t - kT_b) + \pi \sum_{k=1}^{n-(L+1)/2} a_k q(t - kT_b) \\ &= \pi \sum_{k=n-(L+1)/2+1}^{n+(L-1)/2} a_k q(t - kT_b) + \frac{\pi}{2} \sum_{k=1}^{n-(L+1)/2} a_k \end{aligned} \tag{6}$$

From Eq. 6, it can be seen that the phase of GMSK modulating signals can be divided into two parts. Define the first term on the right side of Eq. 6 as the instant phase, which can be written as

$$\psi(t; a_n) = \pi \sum_{k=n-(L+1)/2+1}^{n+(L-1)/2} a_k q(t - kT_b) \tag{7}$$

And define the second term as the accumulative phase

$$\psi_n = \left(\frac{\pi}{2} \sum_{k=1}^{n-(L+1)/2} a_k\right) \bmod (2\pi) \tag{8}$$

From the Eq. 6, the phase function is determined by the phase state at time $t = nT_b$, which is defined as

$$S_n \triangleq \left\{\psi_n, a_{n-\frac{L+1}{2}+1}, a_{n-\frac{L+1}{2}+2}, \ldots, a_{n+\frac{L-1}{2}}\right\} \tag{9}$$

Then, the phase state at time $t = (n+1)T_b$ can be expressed as

$$S_{n+1} = \left\{\psi_{n+1}, a_{n-\frac{L+1}{2}+2}, a_{n-\frac{L+1}{2}+3}, \ldots, a_{n+\frac{L-1}{2}+1}\right\} \tag{10}$$

where,

$$\psi_{n+1} = \left(\psi_n + \frac{\pi}{2} a_{n-\frac{L+1}{2}+1}\right) \bmod (2\pi) \tag{11}$$

In the phase state of GMSK modulating signals, the accumulative phase has four possible values, i.e., 0, $\frac{\pi}{2}$, π, $\frac{3\pi}{2}$. Furthermore, the instant phase is determined by the value of L corresponding symbols. Therefore,

the number of possible phase states at time $t = nT_b$ is 4×2^L.

3 Maximum-likelihood detection

Consider the transmission of AIS baseband signals over AWGN channel. Assuming that the complex envelope of the received signal [9] can be expressed as

$$r(t) = s(t-\tau)e^{j[\varphi(t)+\phi]} + w(t) \tag{12}$$

where $\varphi(t) = 2\pi f_d t$, f_d, and ϕ represent the Doppler frequency offset and the phase offset, τ is the time offset, and $w(t)$ is zero-mean complex Gaussian noise with variance $\sigma_n^2 = N_0/2$.

Assuming that $u(t) = s(t-\tau)e^{j\varphi(t)}$, then Eq. 12 can be rewritten as

$$r(t) = u(t)e^{j\phi} + w(t) \tag{13}$$

For convenience, expressing $u(t)$, $s(t-\tau)$, $\theta(t)$, $r(t)$, $w(t)$, and $\varphi(t)$ in the duration of $nT_b \le t \le (n+1)T_b$ as u_n, s_n, θ_n, r_n, w_n, φ ($\varphi = 2\pi f_d T_b$, indicate the phase shift caused by the Doppler frequency offset in the duration of T_b), respectively, then Eq. 13 can be rewritten as

$$r_n = u_n e^{j\phi} + w_n \tag{14}$$

Based on Maximum-likelihood detection, the probability of the N-length received signal sequence $\boldsymbol{r}$ given N-length sequence $\boldsymbol{u}$ can be expressed as [14]

$$\begin{aligned} p(\boldsymbol{r}|\boldsymbol{u}) &= \int_{-\pi}^{\pi} p(\boldsymbol{r}|\boldsymbol{u},\phi)p(\phi)d\phi \\ &= \frac{1}{\left(2\pi\sigma_n^2\right)^N}\exp\left\{-\frac{\sum_{i=0}^{N-1}\left[|r_{n-i}|^2+|u_{n-i}|^2\right]}{2\sigma_n^2}\right\} \\ &\quad \times I_0\left(\frac{1}{\sigma_n^2}\left|\sum_{i=0}^{N-1} r_{n-i}u_{n-i}^*\right|\right) \end{aligned} \tag{15}$$

where $I_0(x)$ is the zeroth order modified Bessel function of the first kind. Note that $|u_n|^2$ is constant for all phases of GMSK signals and $I_0(x)$ is a monotonically increasing function on its argument, so maximizing $p(\boldsymbol{r}|\boldsymbol{u})$ given $\boldsymbol{u}$ is equivalent to maximizing $\left|\sum_{i=0}^{N-1} r_{n-i}u_{n-i}^*\right|^2$. At this point, let the meaning of u_n, s_n, θ_n, and r_n be unchanged and sample the continuous signals into digital signals.

When $N \ge 2$, $\left|\sum_{i=0}^{N-1} r_{n-i}u_{n-i}^*\right|^2$ can be rewritten as

$$\begin{aligned} \left|\sum_{i=0}^{N-1} r_{n-i}u_{n-i}^*\right|^2 &= \left|\sum_{i=0}^{N-1} r_{n-i}\exp\{-j[\theta_{n-i}+(n-i)\varphi]\}\right|^2 \\ &= \sum_{i=0}^{N-1}|r_{n-i}|^2 + 2\sum_{i=1}^{N-1}\mathrm{Re}\left\{\sum_{m=1}^{i}\left[r_{n-i+m}r_{n-i}^*\right.\right. \\ &\qquad \left.\left.\exp[-j(\theta_{n-i+m}-\theta_{n-i}+m\varphi)]\right]\right\} \\ &= \sum_{i=0}^{N-1}|r_{n-i}|^2 + 2\sum_{i=1}^{N-1}\mathrm{Re}\left\{\sum_{m=1}^{i}\exp(-jm\varphi)\right. \\ &\qquad \left.\left[r_{n-i+m}r_{n-i}^*\exp[-j(\theta_{n-i+m}-\theta_{n-i})]\right]\right\} \end{aligned} \tag{16}$$

where θ_{n-i} is the phase of the GMSK modulating signal at time $(n-i)T_b$.

Since GMSK-modulating signals have constant envelope, the first term on the right hand side of Eq. 16 has no effect on the left hand side. So the optimum reception is equivalent to choosing $\boldsymbol{\theta} = \{\theta_{n-i}\}_{i=0}^{N-1}$ and to maximizing $\sum_{i=1}^{N-1}\mathrm{Re}\left\{\sum_{m=1}^{i}\exp(-jm\varphi)\left[r_{n-i+m}r_{n-i}^*\exp(-j(\theta_{n-i+m}-\theta_{n-i}))\right]\right\}$. It can be readily seen that in $\sum_{i=1}^{N-1}\mathrm{Re}\left\{\sum_{m=1}^{i}\exp(-jm\varphi)\left[r_{n-i+m}r_{n-i}^*\exp(-j(\theta_{n-i+m}-\theta_{n-i}))\right]\right\}$, $r_{n-i+m}r_{n-i}^*$ is the $m(m = 1, \ldots, N-1)$ order differential operation of the received signal and $\theta_{n-i+m} - \theta_{n-i}$ is the increment of the phase of modulating signal. So $\sum_{i=1}^{N-1}\mathrm{Re}\left\{\sum_{m=1}^{i}\exp(-jm\varphi)\left[r_{n-i+m}r_{n-i}^*\exp(-j(\theta_{n-i+m}-\theta_{n-i}))\right]\right\}$ is the optimum judgment formula of N symbols combined differential detection over AWGN channel.

4 Multiple-symbol combined differential detection

According to the optimum judgment formula deduced in the "Maximum-Likelihood Detection" section, we propose a multiple-symbol combined differential detection algorithm. As for the algorithm, when the length of the combined differential symbols is N, the cost function of state S at time nT_b is defined as

$$\lambda_{S,n} = \sum_{i=1}^{N-1}\mathrm{Re}\left\{\sum_{m=1}^{i}\exp(-jm\varphi)\left[r_{n-i+m}r_{n-i}^*\exp\left(-j\left(\theta_{n-i+m,S}-\theta_{n-i,S}\right)\right)\right]\right\} \tag{17}$$

When $N \geq 2$, the cost functions have terms containing $\exp(-jm\varphi)$, and φ will affect the function values for different phase states at time nT_b. So, in order to realize the multiple-symbol combined differential detection, $\exp(-jm\varphi)$ must be compensated in Eq. 17.

4.1 Phase compensation based on combined difference

Assume that the Doppler frequency offset is constant over N symbols, substitute Eq. 14 into the first-order differential term in Eq. 17 and we know that

$$\begin{aligned} r_k r_{k-1}^* \exp[-j(\theta_k-\theta_{k-1})] &= \{\exp[j(\theta_k + k\varphi + \phi)] + w_k\}\{\exp[-j(\theta_{k-1} \\ &\quad +(k-1)\varphi + \phi)] + w_{k-1}^*\}\exp[-j(\theta_k-\theta_{k-1})] \\ &= \exp(j\varphi) + \exp\{j(k\varphi + \phi + \theta_{k-1})\}w_{k-1}^* \\ &\quad + \exp\{-j[(k-1)\varphi + \phi + \theta_k]\}w_k \\ &\quad + w_k w_{k-1}^* \exp[-j(\theta_k-\theta_{k-1})] \end{aligned} \tag{18}$$

The second and third terms on the right hand side of Eq. 18 are independent Gaussian random variables with mean zero. The last term is relatively small compared to the first three under practical value of signal-to-noise ratio (NSNR). So the phase shift at time nT_b, which is caused by the frequency offset in the duration of T_b, can be estimated as

$$e^{j\hat{\varphi}}_n = \frac{1}{n-1}\sum_{k=2}^{n}\left\{r_k r_{k-1}^* \exp[-j(\theta_k-\theta_{k-1})]\right\} \tag{19}$$

Similarly, when it comes to m order difference

$$\begin{aligned} r_k r_{k-m}^* \exp[-j(\theta_k-\theta_{k-m})] &= \{\exp[j(\theta_k + k\varphi + \phi)] + w_k\} \\ &\quad \left\{\exp[-j(\theta_{k-m} + (k-m)\varphi + \phi)] + w_{k-m}^*\right\} \\ &\quad \exp[-j(\theta_k-\theta_{k-m})] \\ &= \exp(jm\varphi) + \exp\{j(k\varphi + \phi + \theta_{k-m})\}w_{k-m}^* \\ &\quad + \exp\{-j[(k-m)\varphi + \phi + \theta_k]\}w_k \\ &\quad + w_k w_{k-m}^* \exp[-j(\theta_k-\theta_{k-m})] \end{aligned} \tag{20}$$

Then, at time nT_b, the estimation of the phase shift caused by the frequency offset in the duration of mT_b is

$$e^{jm\hat{\varphi}}_n = \frac{1}{n-m}\sum_{k=m+1}^{n}\left\{r_k r_{k-m}^* \exp[-j(\theta_k-\theta_{k-m})]\right\} \tag{21}$$

On closer inspection, we know that Eq. 21 can be rewritten into recursive form. So Eq. 21 can be rewritten base on the estimation at time $(n-1)T_b$

$$e^{jm\hat{\varphi}}_n = \frac{1}{n-m}\left\{(n-m-1)e^{jm\hat{\varphi}}_{n-1} + r_k r_{k-m}^* \exp[-j(\theta_k-\theta_{k-m})]\right\} \tag{22}$$

In what follows, applying Eq. 22 to the compensation for $\exp(-jm\varphi)$ in Eq. 17, when $N = 2$, substituting Eq. 22 into Eq. 17 and the cost function of state S at time nT_b is

$$\begin{aligned} \lambda_{S,n} = \mathrm{Re}\Bigg\{\frac{1}{n-1}\Big\{(n-2)e^{j\hat{\varphi}}_{n-1} + r_n r_{n-1}^* \exp[-j(\theta_n-\theta_{n-1})]\Big\}^* \\ r_n r_{n-1}^* \exp[-j(\theta_n-\theta_{n-1})]\Bigg\} \end{aligned} \tag{23}$$

When $N = 3$, the cost function of state S at time nT_b is

$$\begin{aligned} \lambda_{S,n} = \mathrm{Re}\Bigg\{&\frac{1}{n-1}\Big\{(n-2)e^{j\hat{\varphi}}_{n-1} + r_n r_{n-1}^* \exp[-j(\theta_n-\theta_{n-1})]\Big\}^* \\ &\Big\{r_n r_{n-1}^* \exp[-j(\theta_n-\theta_{n-1})] + r_{n-1} r_{n-2}^* \exp[-j(\theta_{n-1}-\theta_{n-2})]\Big\} \\ &+\frac{1}{n-2}\Big\{(n-3)e^{j2\hat{\varphi}}_{n-1} + r_n r_{n-2}^* \exp[-j(\theta_n-\theta_{n-2})]\Big\}^* \\ &r_n r_{n-2}^* \exp[-j(\theta_n-\theta_{n-2})]\Bigg\} \end{aligned} \tag{24}$$

And when $N = 4$, the cost function of state S at time nT_b is

$$\begin{aligned} \lambda_{S,n} = \mathrm{Re}\Bigg\{&\frac{1}{n-1}\Big\{(n-2)e^{j\hat{\varphi}}_{n-1} + r_n r_{n-1}^* \exp[-j(\theta_n-\theta_{n-1})]\Big\}^* \\ &\Big\{r_n r_{n-1}^* \exp[-j(\theta_n-\theta_{n-1})] + r_{n-1} r_{n-2}^* \exp[-j(\theta_{n-1}-\theta_{n-2})] \\ &\quad + r_{n-2} r_{n-3}^* \exp[-j(\theta_{n-2}-\theta_{n-3})]\Big\} \\ &+\frac{1}{n-2}\Big\{(n-3)e^{j2\hat{\varphi}}_{n-1} + r_n r_{n-2}^* \exp[-j(\theta_n-\theta_{n-2})]\Big\}^* \\ &\Big\{r_n r_{n-2}^* \exp[-j(\theta_n-\theta_{n-2})] + r_{n-1} r_{n-3}^* \exp[-j(\theta_{n-1}-\theta_{n-3})]\Big\} \\ &+\frac{1}{n-3}\Big\{(n-4)e^{j3\hat{\varphi}}_{n-1} + r_n r_{n-3}^* \exp[-j(\theta_n-\theta_{n-3})]\Big\}^* \\ &r_n r_{n-3}^* \exp[-j(\theta_n-\theta_{n-3})]\Bigg\} \end{aligned} \tag{25}$$

As can be seen from Eqs. 23, 24, and 25, the phase shift at time nT_b, which is caused by the frequency offset in the duration of mT_b, is estimated from the differential terms in the cost function without introducing any other variables or algorithms.

Above all, as for the multiple-symbol combined differential detection with phase compensation based on combined difference (MSCDD-PCCD), when the length of the combined differential symbols is N, the cost function of state S at time nT_b is

$$\begin{aligned} \lambda_{S,n} &= \sum_{i=1}^{N-1}\mathrm{Re}\left\{\sum_{m=1}^{i}\exp(-jm\varphi)\left[r_{n-i+m} r_{n-i}^* \exp\left(-j\left(\theta_{n-i+m,S}-\theta_{n-i,S}\right)\right)\right]\right\} \\ &= \sum_{i=1}^{N-1}\mathrm{Re}\left\{\sum_{m=1}^{i}\frac{1}{n-m}\left\{(n-m-1)e^{jm\hat{\varphi}}_{n-1} + r_n r_{n-m}^* \exp\left[-j\left(\theta_{n,S}-\theta_{n-m,S}\right)\right]\right\}^* \right. \\ &\qquad \left.\left[r_{n-i+m} r_{n-i}^* \exp\left(-j\left(\theta_{n-i+m,S}-\theta_{n-i,S}\right)\right)\right]\right\} \end{aligned} \tag{26}$$

It can be seen from Eq. 26 that the calculation amount of the MSCDD-PCCD increases multiply with the increases of the length of the combined differential symbols. But the decoding performance gets better and better at the same time, which is shown in the simulation results. Above all, we need to consider both the decoding performance and the calculation amount when we choose the length of the combined differential symbols.

4.2 Phase compensation based on multiple-order combined difference

As mentioned previously in Eqs. 18 and 19, $e_n^{j\hat{\varphi}}$ is the approximation of $e^{j\varphi}$ in the case of statistical average. When the length of the combined differential symbols is $N \geq 3$, we can get more accurate estimation of $e^{j\varphi}$ at time nT_b if we use multiple-order differential information. The estimation of the phase shift caused by the frequency offset in the duration of mT_b in Eq. 21 can be rewritten as

$$e_n^{j\hat{\varphi}} = \frac{1}{n-m}\sum_{k=m+1}^{n}\left\{r_k r_{k-m}^{*}\exp[-j(\theta_k-\theta_{k-m})]\right\}^{\frac{1}{m}} \tag{27}$$

According to Eqs. 19 and 27, the phase shift caused by the frequency offset in the duration of T_b at time nT_b can be estimated as

$$e_n^{j\hat{\varphi}} = \frac{1}{(N-1)n-\left(N^2-N\right)/2}\left\{\left\{(N-1)(n-1)-\left(N^2-N\right)/2\right\}e_{n-1}^{j\hat{\varphi}} + \sum_{m=1}^{N-1}\left\{r_n r_{n-m}^{*}\exp[-j(\theta_n-\theta_{n-m})]\right\}^{\frac{1}{m}}\right\} \tag{28}$$

In what follows, applying Eq. 28 to the compensation for $\exp(-jm\varphi)$ in Eq. 17, when $N = 3$, substituting Eq. 28 into Eq. 17 and the cost function of state S at time nT_b is

$$\begin{aligned}\lambda_{S,n}^{'} = \mathrm{Re}\Bigg\{&\frac{1}{2n-3}\Big\{(2n-5)e_{n-1}^{j\hat{\varphi}} + r_n r_{n-1}^{*}\exp[-j(\theta_n-\theta_{n-1})] \\ &+\left\{r_n r_{n-2}^{*}\exp[-j(\theta_n-\theta_{n-2})]\right\}^{\frac{1}{2}}\Big\}^{*}\Big\{r_n r_{n-1}^{*}\exp[-j(\theta_n-\theta_{n-1})] \\ &+r_{n-1}r_{n-2}^{*}\exp[-j(\theta_{n-1}-\theta_{n-2})]\Big\} \\ &+\Bigg\{\frac{1}{2n-3}\Big\{(2n-5)e_{n-1}^{j\hat{\varphi}} + r_n r_{n-1}^{*}\exp[-j(\theta_n-\theta_{n-1})] \\ &+\left\{r_n r_{n-2}^{*}\exp[-j(\theta_n-\theta_{n-2})]\right\}^{\frac{1}{2}}\Big\}^{*}\Bigg\}^{2} r_n r_{n-2}^{*}\exp[-j(\theta_n-\theta_{n-2})]\Bigg\}\end{aligned} \tag{29}$$

When $N = 4$, the cost function of state S at time nT_b is

$$\begin{aligned}\lambda_{S,n}^{'} = \mathrm{Re}\Bigg\{&\frac{1}{3n-6}\Big\{(3n-9)e_{n-1}^{j\hat{\varphi}} + r_n r_{n-1}^{*}\exp[-j(\theta_n-\theta_{n-1})] \\ &+\left\{r_n r_{n-2}^{*}\exp[-j(\theta_n-\theta_{n-2})]\right\}^{\frac{1}{2}} + \left\{r_n r_{n-3}^{*}\exp[-j(\theta_n-\theta_{n-3})]\right\}^{\frac{1}{3}}\Big\}^{*} \\ &\Big\{r_n r_{n-1}^{*}\exp[-j(\theta_n-\theta_{n-1})] + r_{n-1}r_{n-2}^{*}\exp[-j(\theta_{n-1}-\theta_{n-2})] \\ &+r_{n-2}r_{n-3}^{*}\exp[-j(\theta_{n-2}-\theta_{n-3})]\Big\} \\ &+\Bigg\{\frac{1}{3n-6}\Big\{(3n-9)e_{n-1}^{j\hat{\varphi}} + r_n r_{n-1}^{*}\exp[-j(\theta_n-\theta_{n-1})] \\ &+\left\{r_n r_{n-2}^{*}\exp[-j(\theta_n-\theta_{n-2})]\right\}^{\frac{1}{2}} + \left\{r_n r_{n-3}^{*}\exp[-j(\theta_n-\theta_{n-3})]\right\}^{\frac{1}{3}}\Big\}^{*}\Bigg\}^{2} \\ &\Big\{r_n r_{n-2}^{*}\exp[-j(\theta_n-\theta_{n-2})] + r_{n-1}r_{n-3}^{*}\exp[-j(\theta_{n-1}-\theta_{n-3})]\Big\} \\ &+\Bigg\{\frac{1}{3n-6}\Big\{(3n-9)e_{n-1}^{j\hat{\varphi}} + r_n r_{n-1}^{*}\exp[-j(\theta_n-\theta_{n-1})] \\ &+\left\{r_n r_{n-2}^{*}\exp[-j(\theta_n-\theta_{n-2})]\right\}^{\frac{1}{2}} + \left\{r_n r_{n-3}^{*}\exp[-j(\theta_n-\theta_{n-3})]\right\}^{\frac{1}{3}}\Big\}^{*}\Bigg\}^{3} \\ &r_n r_{n-3}^{*}\exp[-j(\theta_n-\theta_{n-3})]\Bigg\}\end{aligned} \tag{30}$$

Above all, as for the multiple-symbol combined differential detection with phase compensation based on multiple-order combined difference (MSCDD-PCMCD), when the length of the combined differential symbols is N, the cost function of state S at time nT_b is

$$\begin{aligned}\lambda_{S,n}^{'} &= \sum_{i=1}^{N-1}\mathrm{Re}\left\{\sum_{m=1}^{i}\exp(-jm\varphi)\left[r_{n-i+m}r_{n-i}^{*}\exp\left(-j\left(\theta_{n-i+m,S}-\theta_{n-i,S}\right)\right)\right]\right\} \\ &= \sum_{i=1}^{N-1}\mathrm{Re}\left\{\sum_{m=1}^{i}\left\{\frac{\left\{\left\{(N-1)(n-1)-\left(N^2-N\right)/2\right\}e_{n-1}^{j\hat{\varphi}} + \sum_{k=1}^{N-1}\left\{r_n r_{n-k}^{*}\exp\left[-j\left(\theta_{n,S}-\theta_{n-k,S}\right)\right]\right\}^{\frac{1}{k}}\right\}^{*}}{(N-1)n-\left(N^2-N\right)/2}\right\}^{m}\left[r_{n-i+m}r_{n-i}^{*}\exp\left(-j\left(\theta_{n-i+m,S}-\theta_{n-i,S}\right)\right)\right]\right\}\end{aligned} \tag{31}$$

Table 1 All states in the decoding process

State number	All states			
	a_{n-1}	a_n	a_{n+1}	Accumulative phase
1	+1	+1	+1	0
2	+1	+1	−1	0
3	+1	−1	+1	0
4	+1	−1	−1	0
5	−1	+1	+1	0
6	−1	+1	−1	0
7	−1	−1	+1	0
8	−1	−1	−1	0
9	+1	+1	+1	π/2
10	+1	+1	−1	π/2
…	…	…	…	…
28	+1	−1	−1	3π/2
29	−1	+1	+1	3π/2
30	−1	+1	−1	3π/2
31	−1	−1	+1	3π/2
32	−1	−1	−1	3π/2

Comparing Eq. 31 with Eq. 26, it can be seen that the estimation of the phase shift caused by the frequency offset in Eq. 31 is more accurate. Thus, MSCDD-PCMCD has better performance, but its calculation is more complex at the same time.

4.3 Multiple-symbol combined differential Viterbi decoding

According to the cost function of the multiple-symbol combined differential detection, the decoding process adopting Viterbi algorithm can be conducted by regarding the cost function of Eq. 26 or Eq. 31 as the branch metric.

Viterbi algorithm is a kind of search algorithm in trellis which can realize the maximum-likelihood detection of symbol sequence. Every route in the trellis has a corresponding sequence of trellis states, and every sequence of trellis states has a corresponding sequence of symbols, so decoding the symbol sequence with Viterbi algorithm is equivalent to finding an optimum route of trellis states in the trellis. In this paper, we define phase states in Eq. 9 as trellis states in the decoding. When $L = 3$,, the possible states are shown in Table 1.

5 Simulation results

Verification of the proposed algorithm is carried out by comparing the corresponding simulation results in this paper, sampling the received signal at a rate which is eight times to the symbol rate ($R_b = 9.6$ kbps). In order to improve the accuracy of our simulation, we use 1000 symbols in every decoding and take the average BER after repeating 100 times for every NSNR, let $BT = 0.4$ and $L = 3$.

As for the MSCDD-PCCD, when the length of the combined differential symbols is $N = 2, 3, 4, 5$,, they are

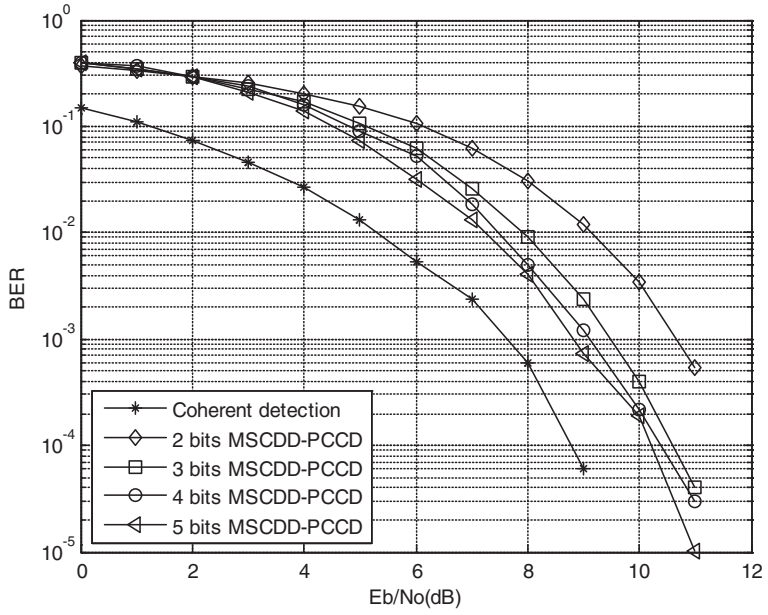

Fig. 1 BER curves of MSCDD-PCCD with different length of combined symbols. The BER of 2 bits MSCDD-PCCD is below 10^{-3} when the NSNR is 11 dB. Additionally, the decoding performances approach those of the coherent detection as the length of the combined differential symbols increases, but the promotion is less and less

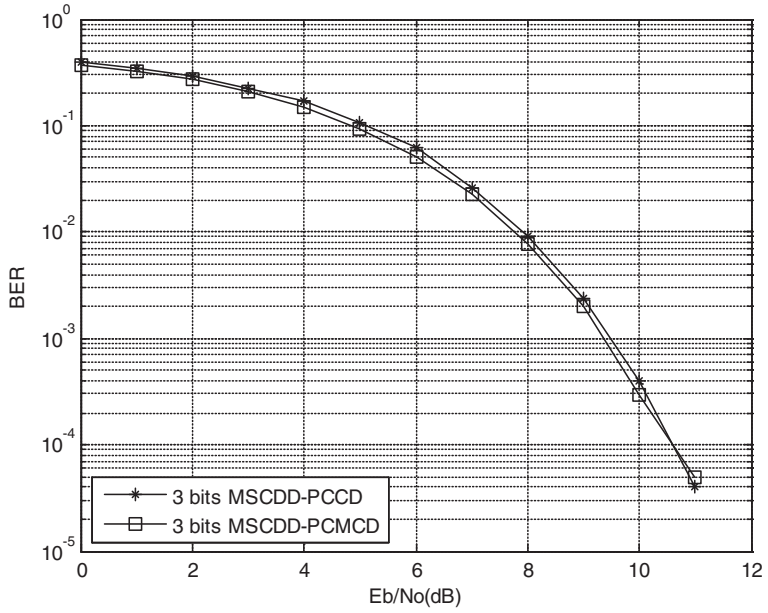

Fig. 2 BER curves of 3 bits MSCDD-PCCD and 3 bits MSCDD-PCMCD. The decoding performances of 3 bits MSCDD-PCMCD and 3 bits MSCDD-PCCD are compared. Three bits MSCDD-PCMCD performs better than 3 bits MSCDD-PCCD

2 bits MSCDD-PCCD, 3 bits MSCDD-PCCD, 4 bits MSCDD-PCCD, and 5 bits MSCDD-PCCD, respectively. Their BER curves together with those of coherent detection are shown in Fig. 1. It can be seen from Fig. 1 that the BER of 2 bits MSCDD-PCCD is below 10^{-3} when the NSNR is 11 dB. Additionally, the decoding performances approach those of the coherent detection as the length of the combined differential symbols increases, but the promotion is less and less.

When the length of the combined differential symbols is $N = 3, 4, 5$, the BER curves of MSCDD-PCCD and MSCDD-PCMCD are shown in Figs. 2, 3, and 4. According

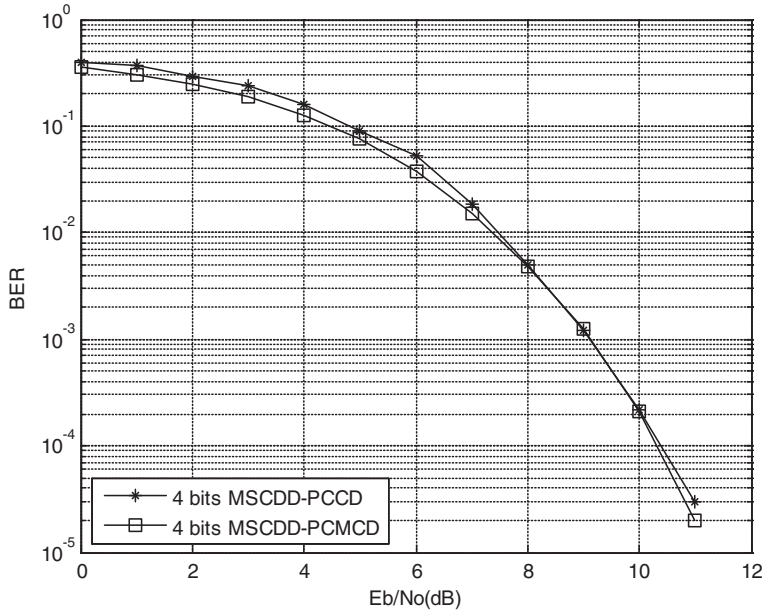

Fig. 3 BER curves of 4 bits MSCDD-PCCD and 4 bits MSCDD-PCMCD. The decoding performances of 4 bits MSCDD-PCMCD and 4 bits MSCDD-PCCD are compared. Four bits MSCDD-PCMCD performs better than 4 bits MSCDD-PCCD

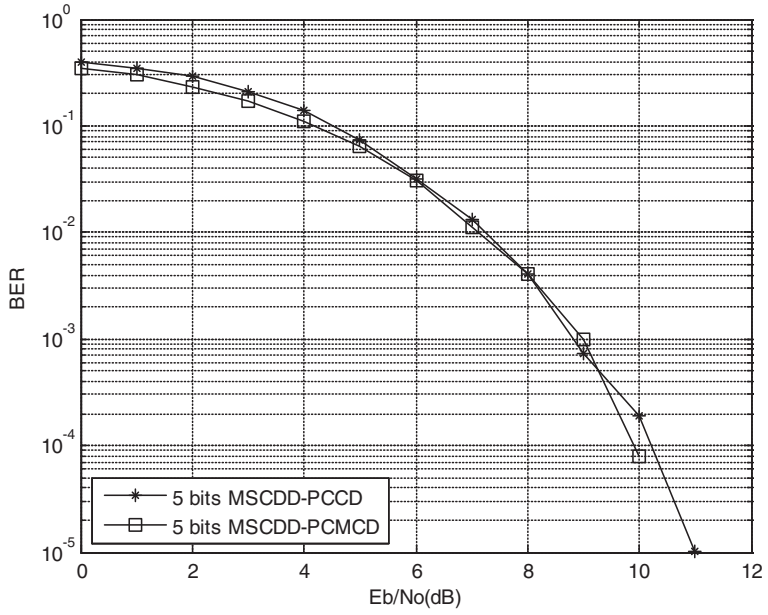

Fig. 4 BER curves of 5 bits MSCDD-PCCD and 5 bits MSCDD-PCMCD. The decoding performances of 5 bits MSCDD-PCMCD and 5 bits MSCDD-PCCD are compared. Five bits MSCDD-PCMCD performs better than 5 bits MSCDD-PCCD

to the results, it is easy to find that with the same length of the combined differential symbols, the MSCDD-PCMCD performs better than the MSCDD-PCCD.

Figure 5 displays the BER curves of 2 bits MSCDD-PCCD and 3 bits MSCDD-PCCD when the phase shifts of received signals are $0, -\frac{2\pi}{3}, -\frac{\pi}{2}, -\frac{\pi}{6}, \frac{\pi}{6}, \frac{\pi}{2}, \frac{2\pi}{3}, \pi$. The decoding performance of 2 bits MSCDD-PCCD and 3 bits MSCDD-PCCD remain unchanged under different phase shifts. So the multiple-symbol combined differential detection algorithm is insensitive to constant phase shift.

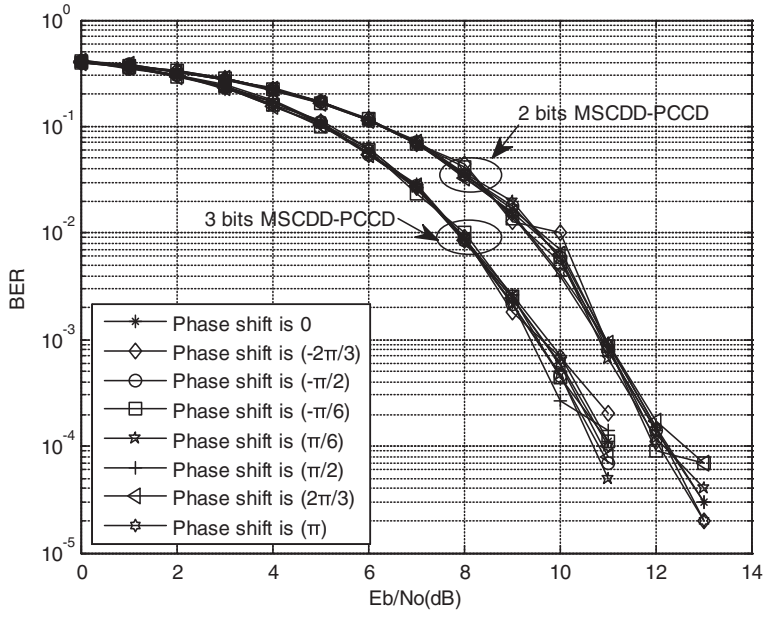

Fig. 5 BER curves of 2 bits MSCDD-PCCD and 3 bits MSCDD-PCCD under different phase shifts. The decoding performance of 2 bits MSCDD-PCCD and 3 bits MSCDD-PCCD remains unchanged when the phase shifts of received signals are $0, -\frac{2\pi}{3}, -\frac{\pi}{2}, -\frac{\pi}{6}, \frac{\pi}{6}, \frac{\pi}{2}, \frac{2\pi}{3}, \pi$

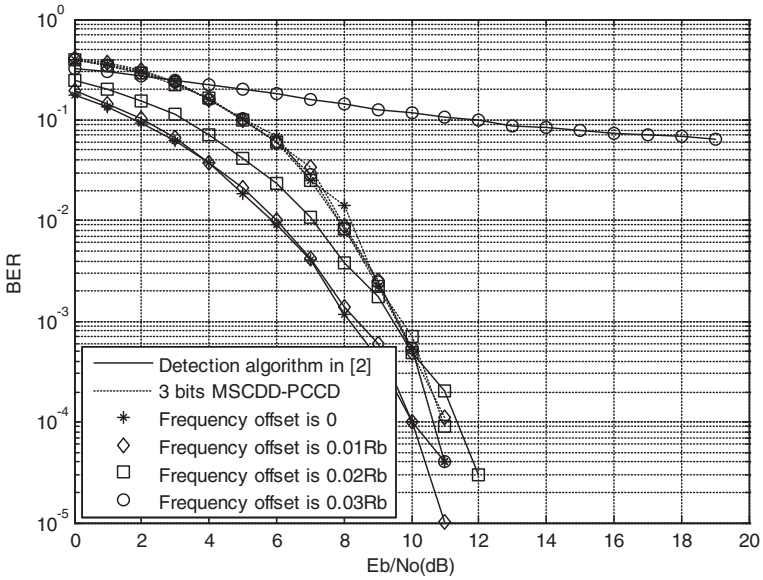

Fig. 6 BER curves of detection algorithm in [2] and 3 bits MSCDD-PCCD under different frequency offsets. The maximum tolerable frequency offset of the detection algorithm in [2] is about $0.02R_b$, while the decoding performances of 3 bits MSCDD-PCCD remain unchanged under different frequency offsets

The BER curves of the detection algorithm in [2] and 3 bits MSCDD-PCCD when the frequency offset of received signals are 0, $0.01R_b$, $0.02R_b$, and $0.03R_b$, respectively, are shown in Fig. 6. And the BER curves of 2 bits MSCDD-PCCD and 3 bits MSCDD-PCCD when the frequency offsets of received signals are 0, $0.01R_b$, $0.10R_b$, $0.26R_b$, and $0.42R_b$, respectively, are shown in Fig. 7. As can be seen in Figs. 6 and 7, the maximum tolerable frequency offset of the detection algorithm in [2] is about $0.02R_b$, while the decoding performances of 2 bits

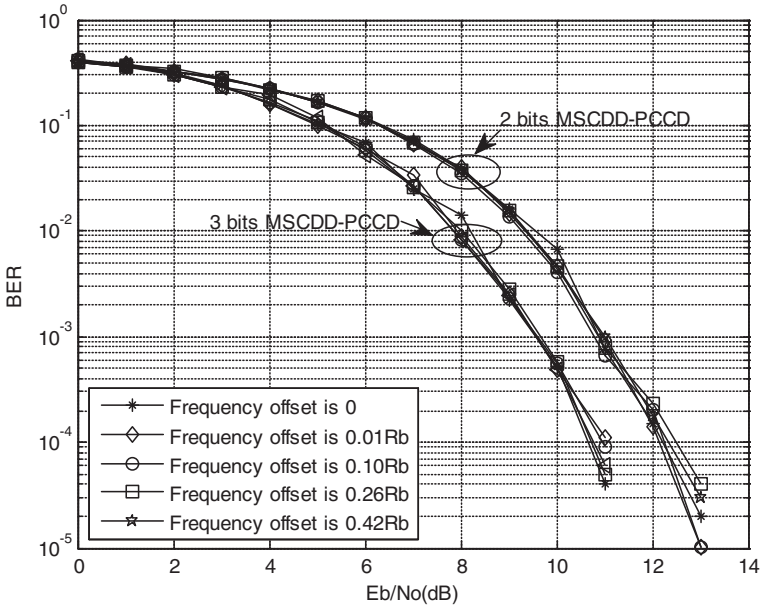

Fig. 7 BER curves of 2 bits MSCDD-PCCD and 3 bits MSCDD-PCCD under different frequency offsets. The decoding performance of 2 bits MSCDD-PCCD and 3 bits MSCDD-PCCD remains unchanged when the frequency offsets of received signals are 0, $0.01R_b$, $0.10R_b$, $0.26R_b$, $0.42R_b$ respectively

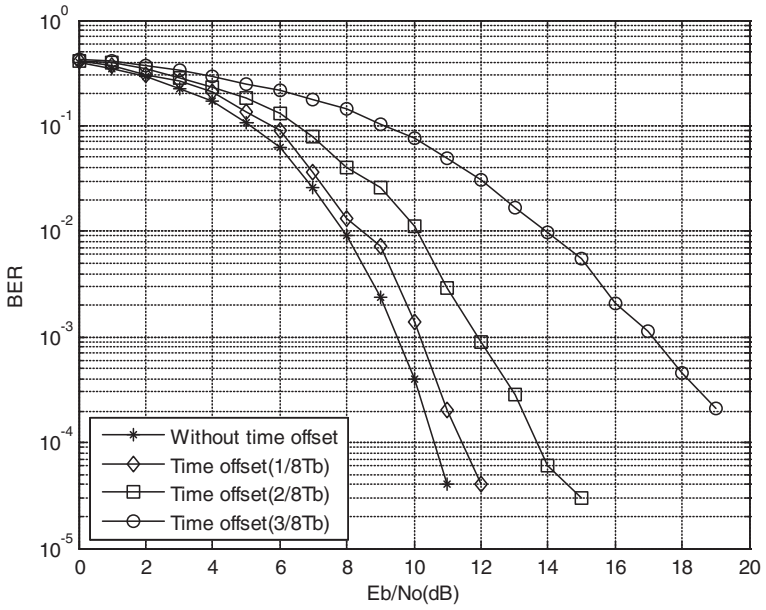

Fig. 8 BER curves of 3 bits MSCDD-PCCD with various time offsets. The decoding performances of 3 bits MSCDD-PCCD get worse and worse when the time offset increases. So we need to do time recovery before the application of this method in the receiver

MSCDD-PCCD and 3 bits MSCDD-PCCD remain unchanged under different frequency offsets. So the receiver in [2] needs carrier frequency recovery algorithm to lower the frequency offset to at most $0.02R_b$. The receiver in [9] needs frequency synchronization algorithm too. But the proposed algorithm makes compensation for the phase shift caused by the frequency offset from the multiple-order combined differential information in the process of decoding, so there is no need for frequency recovery algorithm in the receiver.

Figure 8 shows the BER curves of 3 bits MSCDD-PCCD with various time offsets. The decoding performances of 3

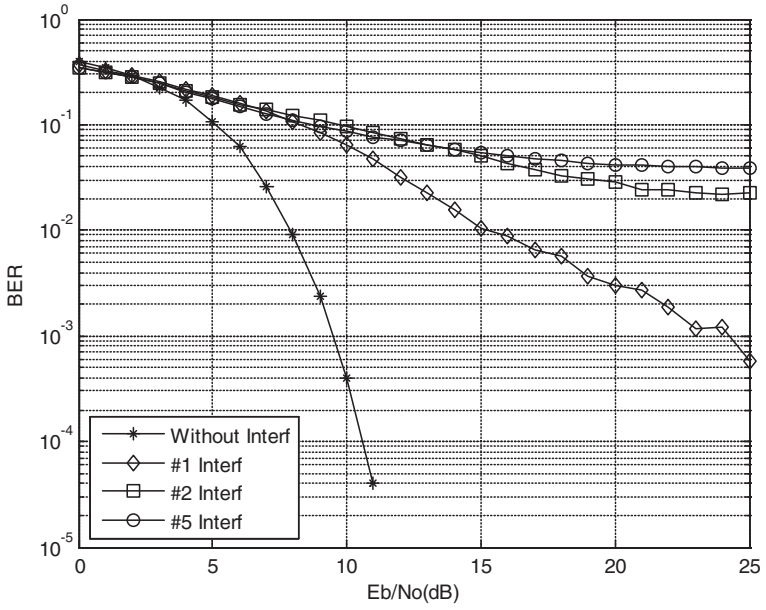

Fig. 9 BER curves of 3 bits MSCDD-PCCD with various numbers of interfering signals and total C/I = 5 dB. The BER of 3 bits MSCDD-PCCD can reach 10^{-2} with one interfering signal when the NSNR is 15 dB. So the decoding of messages colliding with a relatively low C/I is still possible provided the NSNR is high enough

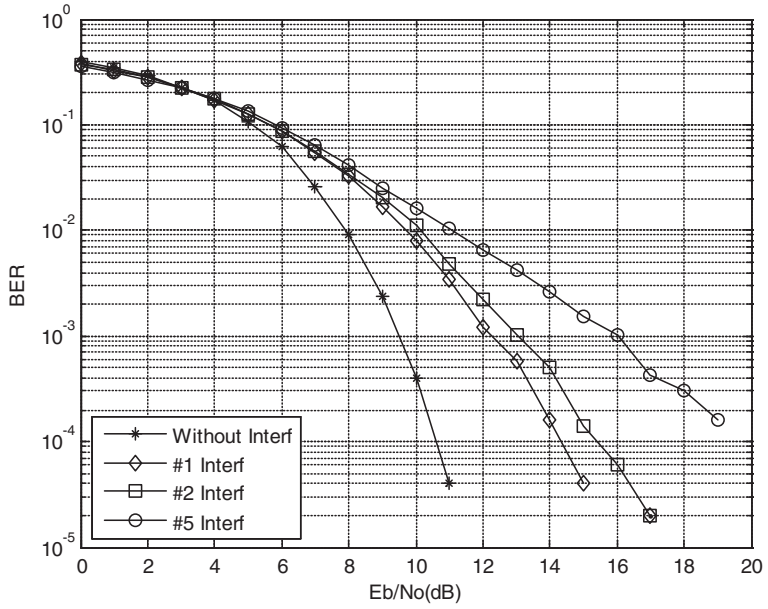

Fig. 10 BER curves of 3 bits MSCDD-PCCD with various numbers of interfering signals and total C/I = 10 dB. The decoding performances deteriorate with the number of interfering signals increases under the same C/I

bits MSCDD-PCCD get worse and worse when the time offset increases. So we need to do time recovery as described in [15] before the application of the proposed algorithm in the receiver.

Figures 9 and 10 show the BER curves of 3 bits MSCDD-PCCD with a variable number of interfering signals when the C/I (signal-to-overall-interference power ratio) is 5 dB and 10 dB. It can be seen in Fig. 9 that the BER of 3 bits MSCDD-PCCD can reach 10^{-2} with one interfering signal when the NSNR is 15 dB. So the decoding of messages colliding with a relatively low C/I is still possible provided the NSNR is high enough [2]. And the decoding performances deteriorate with the number of interfering signals increase under the same C/I.

6 Conclusions

In this paper, a multiple-symbol combined differential Viterbi algorithm for the detection of satellite-based AIS signals is proposed. This algorithm combines the multiple-order combined differential information with the Viterbi algorithm according to the theories of multiple-symbol differential detection and maximum-likelihood detection. The phase shift caused by the frequency offset is estimated and compensated from the above information in the process of decoding. The proposed algorithm performs well under low NSNR, and the decoding performances approach those of the coherent detection as the length of the combined differential symbols increases. Most importantly, its performance remains stable under different frequency offsets, which is attractive for the detection of signals with large Doppler frequency offsets.

Competing interests

The authors declare that they have no competing interests.

Acknowledgements

This work was supported by the National Natural Science Foundation of China (No. 61371108), Tianjin Research Program of Application Foundation and Advanced Technology (No. 15JCQNJC01800), and Tianjin City High School Science & Technology Fund Planning Project (Nos. 20140706 and 20140707).

Received: 19 January 2015 Accepted: 13 July 2015
Published online: 30 July 2015

References

1. International Telecommunication Union, *Technical characteristics for an automatic identification system using time division multiple access in the VHF maritime mobile frequency band. Recommendation ITU-R M*, 2014, pp. 1371–5
2. P Burzigotti, A Ginesi, G Colavolpe, Advanced receiver design for satellite-based automatic identification system signal detection. Int J Satellite Comm Networking **30**(2), 52–63 (2012)
3. P Mathieu, O Mohamed Rabie, F Grégory, H Sébastien, *An adaptive multi-user multi-antenna receiver for satellite-based AIS detection*. 2012 6th Advanced Satellite Multimedia Systems Conference (ASMS) and 12th Signal Processing for Space Communications Workshop (SPSC), 2012, pp. 273–280
4. P Timothy, CW Bostian, JE Allnutt. Satellite Communications. 2nd Edition, Publishing House of Electronics Industry, John Wiley & Sons, 2003.
5. C Giulio, R Riccardo, Noncoherent sequence detection of continuous phase modulations. IEEE Trans Commun **47**(9), 1303–1307 (1999)
6. M Dimitrios, F Kamilo, Multiple differential detection of continuous phase modulation signals. IEEE Trans Veh Technol **42**(2), 186–196 (1993)
7. A Abrardo, G Benelli, GR Cau, Multiple-symbol differential detection of GMSK for mobile communications. IEEE Trans Veh Technol **44**(3), 379–389 (1995)

8. H Mathis, Differential detection of GMSK signals with low B_tT using the SOVA. IEEE Trans Commun **46**(4), 428–430 (1998)
9. G Colavolpe, T Foggi, A Ugolini, J Lizarraga, S Cioni, and A Ginesi. A highly efficient receiver for satellite-based automatic identification system signal detection. International Journal of Satellite Communications and Networking. John Wiley & Sons, (2014), doi:10.1002/sat.1095
10. JL Buetefuer, WG Cowley, *Frequency offset insensitive multiple symbol detection of MPSK*. IEEE International Conference on Proceedings, 2000, pp. 2669–2672
11. R Amir Masoud, NC Beaulieu, *Multiple symbol differential detection of MPSK in the presence of frequency offset*. IEEE International Conference on Communications, 2005, pp. 693–697
12. C Giulio, R Riccardo, Detection of linear modulations in the presence of strong phase and frequency instabilities. IEEE Trans Commun **50**(10), 1617–1626 (2002)
13. JG Proakis, *Digital communications*, 4th edn. (McGraw-Hill, New York, 2000)
14. D Dariush, MK Simon, Multiple-symbol differential detection of MPSK. IEEE Trans Commun **38**(3), 300–308 (1990)
15. M Morelli, U Mengali, Joint frequency and timing recovery for MSK-type modulation. IEEE Trans Commun **47**(6), 938–946 (1999)